Doppler-Based Satellite-Borne Localization of Ground Electromagnetic Interferer

Yimin D. Zhang
Department of Electrical and Computer Engineering, Temple University, Philadelphia, PA 19122
ydzhang@temple.edu

Yanwu Ding
Department of Electrical and Computer Engineering, Wichita State University, Wichita, KS 67260
yanwu.ding@wichita.edu

Khanh Pham
Air Force Research Laboratory, Kirtland Air Force Base, NM 87117
khanh.pham.1@spaceforce.mil

Dan Shen
Intelligent Fusion Technology, Inc., Germantown, MD 20876
dshen@intfusiontech.com

Genshe Chen
Intelligent Fusion Technology, Inc., Germantown, MD 20876
gchen@intfusiontech.com

Abstract— **Accurate localization and effective suppression of ground electromagnetic interference (EMI) signals are critical to maintaining uninterrupted satellite operations and the quality of services. For EMI sources emitting certain waveforms, such as continuous-wave or phase shift keying signals, their localization exploiting the time-varying Doppler signature due to satellite motion is an attractive approach. The high-speed motions and complicated orbits of satellites render the Doppler signatures varying with a high dynamic range and nonlinear instantaneous frequency signatures. As such, their processing requires high complexity which may not be practical for real-time processing, particularly for on-orbit satellite implementation for which the computational capability is highly limited. In this paper, we develop a low-complexity approach to iteratively estimate both the location and Doppler signatures of EMI signals. We introduce virtual ground references around the sensed scenarios and compute the Doppler difference between the measured results and the predicted ones for the virtual ground reference positions. By considering such Doppler difference in lieu of the Doppler frequencies, the Doppler dynamic range and the slope of the instantaneous frequency signatures are reduced to facilitate more effective time-frequency analysis and EMI source localization. We further consider the use of multiple virtual ground references for performance improvement, and a simple EMI localization approach is proposed through the interpolation of the Doppler difference frequencies observed at these virtual references. The effectiveness of the proposed approach is verified using simulation results.**

TABLE OF CONTENTS

1. INTRODUCTION

Accurate localization and effective suppression of electromagnetic interference (EMI) sources is important in satellite communications to ensure uninterrupted services. EMI signals can significantly interfere with the operation of the satellite communication system. One effective approach to localize EMI sources is based on the estimated Doppler signatures, particularly when the EMI sources emit continuous-wave (CW) and phase shift keying (PSK) signals [1, 2]. The Doppler frequencies associated with the received EMI signals rapidly vary over time as the satellite moves on its orbit, providing sufficient information for the localization of EMI sources by a single satellite. This contrasts with other methods, such as those based on time difference-of-arrival (TDOA) and frequency difference-of-arrival (FDOA) [3, 4], which require multiple satellites and, therefore, do not apply when only a single satellite is available.

Because a satellite moves on an elliptical orbit at a high speed, the Doppler frequency corresponding to the EMI signals emitted from a stationary ground source is characterized by a highly nonlinear frequency-modulated (FM) signature. While several methods exist to analyze high-order FM signals (e.g., [5–9]), they require high complexity and thus are impractical for real-time processing, particularly for on-orbit satellite implementation for which the computational capability is highly limited. Therefore, the time-frequency analysis in this paper will be primarily based on the simpler form of short-time Fourier transform (STFT) [10]. A challenge in applying STFT is that the window size over which the data can be coherently processed is limited to the applicable time period where the Doppler frequency can be treated as stationary.

To effectively reduce the dynamic range and the slope of the Doppler signatures, in this paper, we introduce a virtual ground reference (VGR) near the actual EMI source by taking advantage of the fact that coarse knowledge of the EMI source is often available through, for example, the directional beams used in satellite communication links [11, 12]. It is emphasized that the VGRs do not physically exist and do not introduce any additional hardware cost. By computing the Doppler frequency

979-8-3503-0462-6/24/$31.00 ©2024 IEEE

associated with a CW signal at the assumed VGR position, the Doppler difference frequency between the EMI source and the VGR can be computed. As the VGR can be assumed reasonably close to the true EMI source position, the Doppler difference frequency changes much slower with a smaller dynamic, thereby facilitating reduced-rate processing of the time-frequency analysis and with a much longer window. As such, the knowledge of a coarse EMI source location enables effective Doppler signature stationarization and, thereby, enables enhanced Doppler analysis and achieves higher robustness against noise [13–15]. As a result, we can improve the accuracy and efficiency of EMI source localization in the underlying single-satellite communications systems. In addition, by utilizing multiple VGR positions and fusing the results using proper weights according to the reliability of each individual estimate, the proposed method would lead to robust localization of low-power EMI sources.

The signal model and problem statement are presented in Section 2. Section 3 describes the VGR-based approach for the estimation of Doppler difference and the localization of EMIs, whereas EMI localization exploiting multiple VGRs is considered in Section 4. Section 5 presents simulation results, and Section 6 draw conclusions of this paper.

Notations: We use lower-case bold characters to describe vectors. $(\cdot)^T$ denotes the transpose of a vector, and $|\cdot|$ denotes the norm of a vector.

2. Signal Model and Problem Statement

We consider the EMI source localization problem as illustrated in Fig. 1, where a single satellite moves on its orbit and localizes a ground EMI emitter based on the detected Doppler signatures estimated from different orbit positions of the satellite. For simplicity and without loss of generality, we consider a single EMI transmitting a CW waveform. The proposed technique can be extended to M-ary PSK signals as these signals can be converted to CW waveforms [16].

Geometrical Model

For simplicity and without loss of generality, we consider the satellite orbit in a simplified two-dimensional (2-D) model in the x-z plane. Denote the location of the stationary EMI as vector $\boldsymbol{x}_e = [x_e, z_e]^T$, and that of the satellite at time instant t as $\boldsymbol{x}_s(t) = [x_s(t), z_s(t)]^T$. The instantaneous velocity vector of the satellite at time t is denoted as $\boldsymbol{v}(t) = [v_x(t), v_z(t)]^T$. We consider a constant scalar velocity of the satellite, but the direction of $\boldsymbol{v}(t)$ is time-varying as satellite moves on its elliptic orbit.

The distance between the satellite and the EMI at time instant t is expressed as

$$D_{es}(t) = |\boldsymbol{x}_s(t) - \boldsymbol{x}_e| = [(x_s(t) - x_e)^2 + (z_s(t) - z_e)^2]^{1/2}. \quad (1)$$

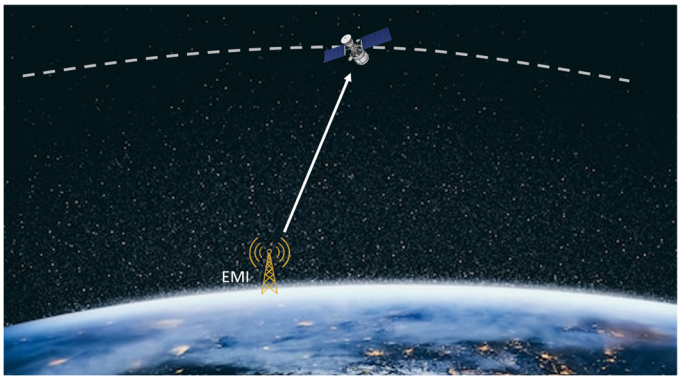

Figure 1. Satellite interfered with a ground EMI emitter.

Denote the CW signal emitted from the EMI as

$$s(t) = A \cdot \exp(j2\pi f_c t), \quad (2)$$

where A is the signal amplitude and f_c is the carrier frequency. Then, the signal received at the satellite is expressed as

$$u(t) = A \cdot \xi(t) \cdot \exp(j2\pi f_c(t - \tau_{es}(t))), \quad (3)$$

where $\xi(t)$ reflects the propagation loss and $\tau_{es}(t) = D_{es}(t)/c$ is the propagation delay, with c denoting the propagation velocity of electromagnetic waves. Note that the effect of ionospheric delays is ignored.

The instantaneous Doppler frequency is obtained as

$$f_{D,es}(t) = -\frac{1}{\lambda} \cdot \frac{\mathrm{d}D_{es}(t)}{\mathrm{d}t} = -\frac{1}{\lambda} \cdot \boldsymbol{v}^T(t)\bar{\boldsymbol{r}}_{es}(t), \quad (4)$$

where $\bar{\boldsymbol{r}}_{es}(t) = \boldsymbol{r}_{es}(t)/|\boldsymbol{r}_{es}(t)|$ is the unit vector associated with $\boldsymbol{r}_{es}(t)$, the vector in the direction from the EMI and the satellite.

Because a satellite moves on an elliptical orbit with a high speed, the Doppler frequency corresponding to the CW signals from the stationary ground EMI source is characterized as a highly nonlinear FM signature. For parameters depicted in Table 1, Fig. 2 shows the Doppler frequency observed for a time period of 100 s. Note that the Doppler frequency is proportional to the carrier frequency, which is assumed to be 4.5 GHz in this paper. The Doppler frequency changes in a different rate at different satellite positions.

Considering the satellite coverage, the maximum Doppler frequency due to the satellite motion is approximately 60 kHz, and we process the baseband signal at a sampling frequency of $f_s = 120$ kHz. As such, the time-varying Doppler frequency is obtained by performing the time-frequency analysis over a series of time samples at $t, t + \Delta, \ldots, t + (M-1)\Delta$, where M is the number of time samples available for coherent processing and the sampling interval is $\Delta = 1/f_s = 8.33$ μs.

Doppler Frequency Analysis

Because of the long distance between the satellite and the earth ground, satellite communications are operated in a very low signal-to-noise ratio (SNR). In this case, low-power EMI sources can interrupt the satellite communication links. In a time-varying scenario with a short coherent time, an accurate estimation of the instantaneous Doppler frequency of the EMI and, subsequently, the location of the EMI become challenging.

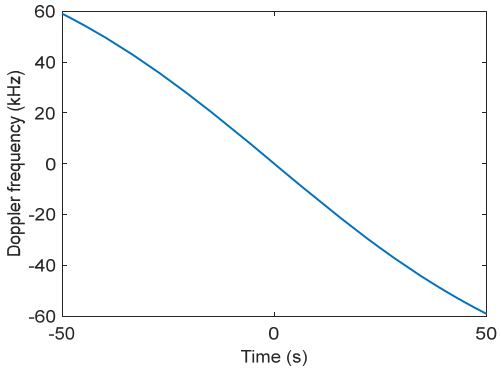

Figure 2. Doppler signature of the EMI signal due to satellite motion.

Table 1: Parameters used in the simulations

Parameter	Value
Satellite altitude	600 km
Satellite speed	7,800 m/s
Frequency	4.5 GHz
EMI position	(0, 0) km

Fig. 3 illustrates the spectrogram, which is the magnitude squared of the STFT, for four different Hamming window sizers of 2,048 points (0.0171 s), 4,096 points (0.0341 s), 8,192 points (0.0683 s), and 16,384 points (0.1365 s), where the input interference-to-noise ratio (INR) is -20 dB. In each subplot, the left panel shows the spectrogram for the 20-second window between 0 s and 20 s. For better visualization, a 1-second window view between 10 s and 11 s is shown at the right panel. The spectrogram is normalized by the peak value and is shown in dB scale with a dynamic range of 40 dB. The number of frequency points is 2^{13} = 8,192, rendering the frequency resolution to be 14.65 Hz. The STFT results are decimated by a factor of 500 in the time axis to reduce the computational complexity.

3. VGR-Based EMI Localization

Now we consider the use of a VGR which is close to the EMI source, as shown in Fig. 4. Denoting the location vector of the

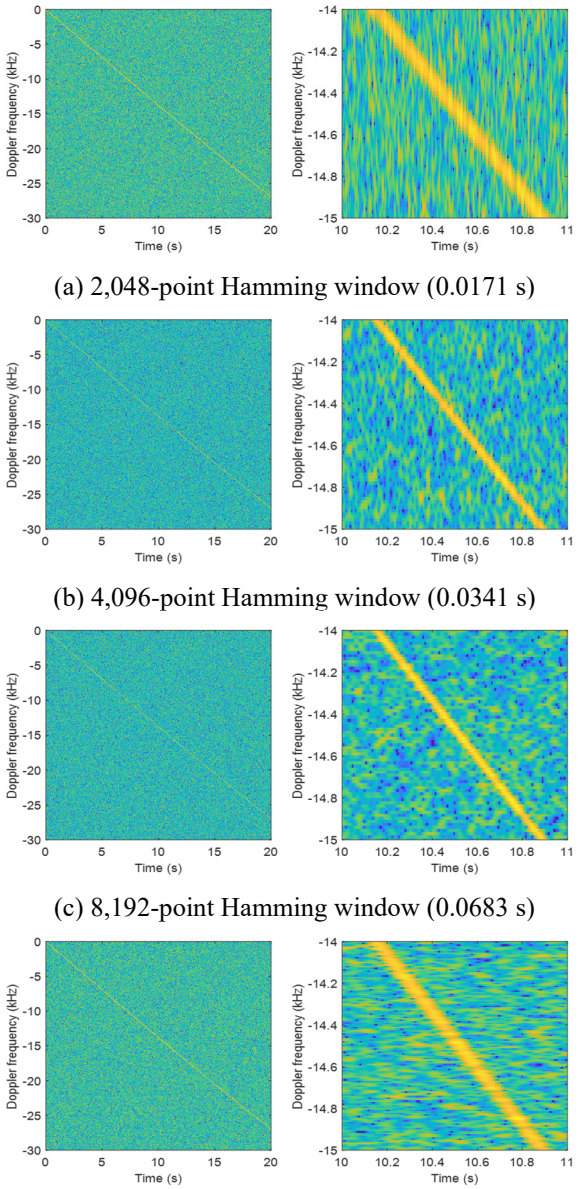

(a) 2,048-point Hamming window (0.0171 s)

(b) 4,096-point Hamming window (0.0341 s)

(c) 8,192-point Hamming window (0.0683 s)

(d) 16,384-point Hamming window (0.1365 s)

Figure 3. Spectrogram of the Doppler signature with different window sizes.

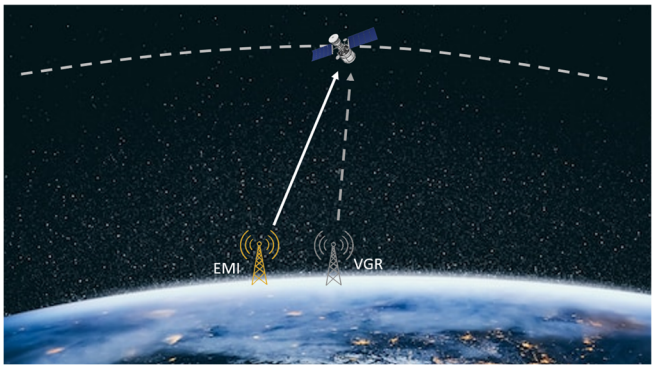

Figure 4. Geometrical presentation of VGR-based approach.

VGR as $\boldsymbol{x}_v = [x_v, z_v]^T$, the distance between the VGR and the satellite at time instant t is expressed as

$$\begin{aligned} D_{vs}(t) &= |\boldsymbol{x}_s(t) - \boldsymbol{x}_v| \\ &= [(x_s(t) - x_v)^2 + (z_s(t) - z_v)^2]^{1/2}. \end{aligned} \tag{5}$$

Similarly, the corresponding instantaneous Doppler frequency corresponding to the time-varying distance is

$$f_{D,vs}(t) = -\frac{1}{\lambda} \cdot \frac{\mathrm{d}D_{vs}(t)}{\mathrm{d}t} = -\frac{1}{\lambda} \cdot \boldsymbol{v}^T(t)\bar{\boldsymbol{r}}_{vs}(t), \tag{6}$$

where $\bar{\boldsymbol{r}}_{vs}(t) = \boldsymbol{r}_{vs}(t)/|\boldsymbol{r}_{vs}(t)|$ with $\boldsymbol{r}_{vs}$ denoting the vector connecting the VGR and the satellite. Based on $f_{D,es}(t)$ and $f_{D,vs}(t)$, we compute the Doppler difference frequency between them as

$$\begin{aligned} \Delta f_D(t) &= f_{D,es}(t) - f_{D,vs}(t) \\ &= -\frac{1}{\lambda} \cdot \frac{\mathrm{d}[D_{es}(t) - D_{vs}(t)]}{\mathrm{d}t} \\ &= -\frac{1}{\lambda} \cdot \boldsymbol{v}^T(t)[\bar{\boldsymbol{r}}_{es}(t) - \bar{\boldsymbol{r}}_{vs}(t)] \approx \frac{\boldsymbol{v}^T(t)\boldsymbol{r}_{ev}}{\lambda|\boldsymbol{r}_{es}(t)|}, \end{aligned} \tag{7}$$

where $\boldsymbol{r}_{ev}$ is a vector connecting the EMI and the VGR which is fixed for a stationary EMI. The last approximation in equation (7) is obtained by assuming $|\boldsymbol{r}_{es}(t)| \approx |\boldsymbol{r}_{vs}(t)|$. The Doppler difference frequency clearly depends on the relative position between the VGR and the EMI. The resulting Doppler difference frequency is negative if the angle between $\boldsymbol{v}^T(t)$ and $\boldsymbol{r}_{ev}$ is less than 90^o. Specifically, when the positions of the VGR and the EMI overlap, Δf_D will become 0.

Consider, for example, $x_v = 20$ km, the Doppler signatures corresponding to the EMI and the VGR are compared in Fig. 5(a). It is clear that these Doppler frequencies are close and vary in a similar manner, rendering a small value of the Doppler difference frequency, as shown in Fig. 5(b). The dynamic range of the Doppler difference frequency is much lower than the Doppler frequency, making it possible to reduce the data rate and exploit a longer window size when computing the STFT. While the signal corresponding to the Doppler difference frequency can be decimated without aliasing in this stage, we keep the same data rate for easier performance comparison, and the window length is set to 2^{20} = 1,048,576 samples (8.74 s). The negative Doppler difference frequency between them indicates that the VGR lies in the position direction of the satellite motion.

Fig. 6 compares the spectrogram of the Doppler frequency of the EMI signal and the Doppler difference frequency between those of the EMI and the VGR. To clearly show the advantage of using the Doppler difference frequency, we used a low input INR of -30 dB in this figure. In this case, the Doppler frequency becomes difficult to identify, whereas the Doppler difference frequency, because of its slowly time-varying characteristics, can still be clearly identified.

Furthermore, because of the relative stationarity of the resulting Doppler difference frequency, we can obtain the averaged spectrum by averaging the obtained spectrogram over a selected observation time period. For example, the average of the spectrogram depicted in Fig. 6(b) over the time period between 0 s and 20 s renders the spectrum showing in Fig. 7, where the peak value indicates the corresponding Doppler difference frequency to be $\hat{f}_{D,vs} = -3.89648$ kHz.

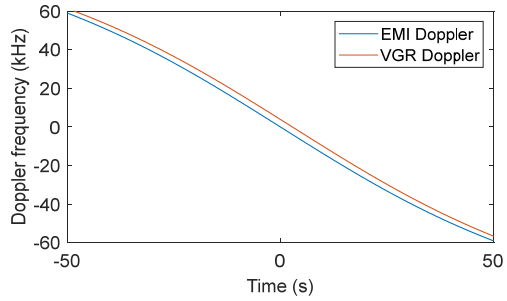

(a) Doppler frequencies of the EMI and VGR signals

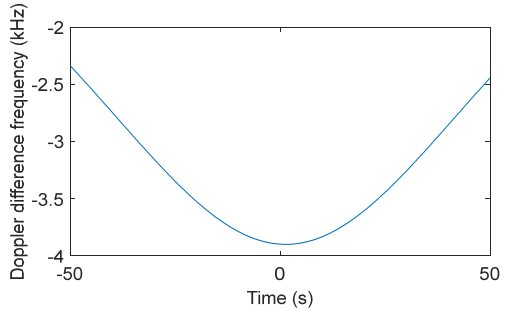

(b) Doppler difference frequency

Figure 5. $

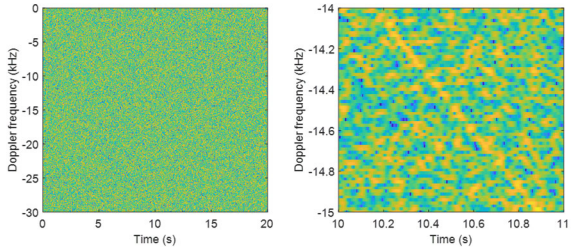

(a) Doppler frequency

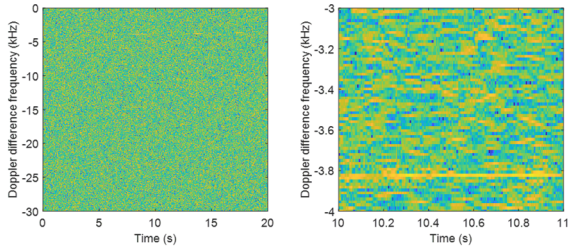

(b) Doppler difference frequency

Figure 6. Spectrogram of the Doppler frequency and Doppler difference frequency (input INR = -30 dB, $x_v = 20$ km).

Once the Doppler difference frequency is identified, the EMI

location can be estimated from the relationship depicted in equation (7). While accurate EMI localization requires the terrain heights to be taken into account, here we consider a flat ground surface model. By ignoring the effect of z-axis motion of the satellite to the Doppler difference frequency, the x-axis position of the EMI can be approximately obtained from the averaged Doppler difference frequency $\Delta\hat{f}_{D,vs}$ as

$$\hat{x}_e \approx x_v + \frac{\lambda \cdot |\boldsymbol{r}_{vs}(t)|}{v_x(t)} \Delta\hat{f}_{D,vs}(t). \tag{8}$$

Using the above estimated value of $\hat{f}_{D,vs}(t) = -3.89648$ kHz, the x-axis position of the EMI is estimated as $\hat{x}_e = -59.4$ m, which is very close to the true EMI source position at $x_e = 0$ m.

4. EMI Localization Exploiting Multiple VGRs

By considering multiple VGRs, we can obtain multiple Doppler difference frequencies. As an example, Fig. 8 shows the Doppler frequencies and the Doppler difference frequency when the VGR is located at $x_v = -30$ km. Such position renders a positive Doppler difference frequency, and its value is roughly proportional to the distance between the VGR and the EMI.

The spectrogram obtained in this case is shown in Fig. 9, and the averaged spectrum magnitude is shown in Fig. 10. Note that, compared to the scenario considered in Section III, the distance between the VGR and the EMI source is larger, and the Doppler difference frequency has a slighter higher slope. As a result, the averaged spectrum magnitude shows a lower value but still provides clear estimation of $\hat{f}_{D,vs} = 5.83008$ kHz. Substituting this result to equation (8) yields an estimated position of the EMI source as $\hat{x}_e = 278.8$ m.

As these examples indicate, the spectrum magnitude typically takes a higher value when the VGR is closer to the EMI source. As such, when interpolating the estimated EMI source position, we can use higher weights towards these estimates, whereas unreliable results must be excluded from consideration. One choice is to use the softmax function, which defines the weight towards the estimated EMI position from the kth VGR as

$$w_k = \frac{e^{\alpha M_k}}{\sum_{l=1}^{K} e^{\alpha M_l}} \tag{9}$$

for $k = 1, \ldots, K$, where $M_k = \widetilde{M}_k - \mu_k$, $\widetilde{M}_k$ is the peak value of the spectrum magnitude of the kth estimate, μ_k is the averaged value across all considered Doppler difference frequency bins, and K is the number of VGRs being considered. In addition, α is a constant introduced to adjust the sensitivity, and $\alpha = 10$ is used in this paper. Based on the two VGR positions considered in Figs. 7 and 10, the estimated EMI source position becomes

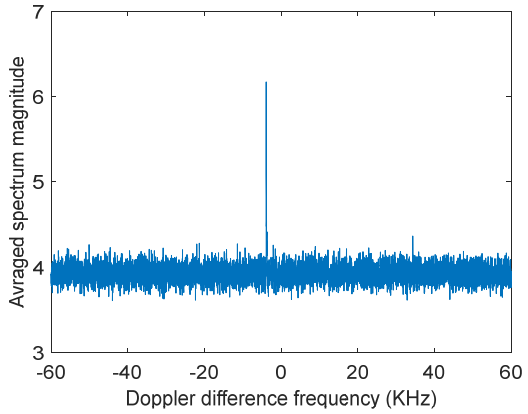

Figure 7. Averaged spectrum of the Doppler difference frequency (input INR = -30 dB, $x_v = 20$ km).

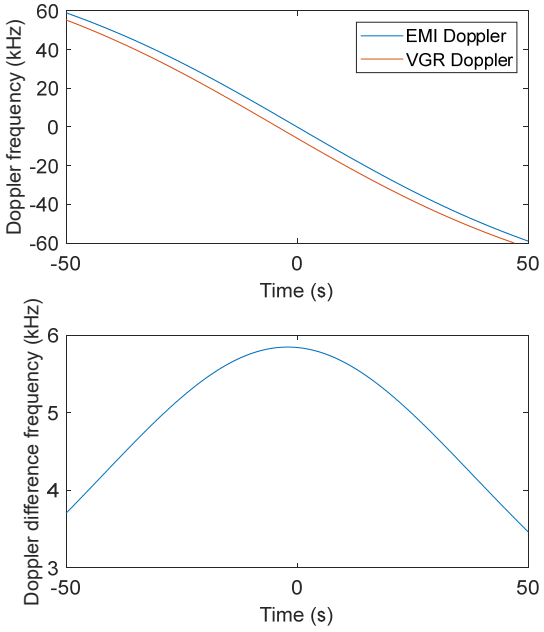

Figure 8. Doppler frequency and Doppler difference frequency ($x_v = -30$ km).

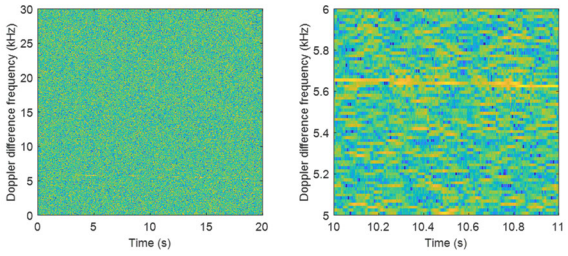

Figure 9. Spectrogram of the Doppler difference frequency (input INR = -30 dB, $x_v = -30$ km).

$\hat{x}_e = -59.3$ m. This result is effectively the same as that obtained from the VGR at $x_v = 20$ km because the result obtained from the other VGR is less reliable.

5. Simulation Results

In this section, we provide EMI localization results for a single VGR case with different input INR levels and VGR locations, and the fused results based on multiple VGRs randomly distributed over a region. For each input INR level, 5 random trials are computed.

Fig. 11 shows the estimated EMI source position with respect to the VGR position and the input INR. White cells indicate that most trials yield successful estimation, and the numbers show the estimated source positions. On the other hand, gray cells denote that most trials fail to provide an accurate estimation. It is seen that, as the VGR departs away from the true EMI source position, a higher value of the input INR is needed to achieve accurate EMI source localization because the Doppler difference frequency is less concentrated. Note also that the results are asymmetrical because they are obtained using the date corresponding to the time period between 0 s and 20 s.

Fig. 12 shows the estimated EMI source location using 9 VGRs located at $[-80, -60, -40, -20, 0, 20, 40, 60, 80]$ km positions. For each input INR level, 5 random trials are carried out. The estimation results become stable when the input INR is -37.5 dB, and a higher accuracy is achieved when the input is -35 dB (less than 5 m error) or above (around 1 m error). Note that direct STFT computation of the Doppler frequency does not provide meaningful Doppler signature estimation and EMI localization when the input INR is -30 dB or lower.

6. Conclusion

We have considered the EMI source localization problem in a single-satellite communication system. The proposed technique is based on the time-frequency analysis of the Doppler signatures due to satellite motion, and VGRs are introduced to stationarize the Doppler frequencies. Based on the coarse knowledge of the EMI positions through beam-based satellite communications, the proposed technique facilitates simplified Doppler difference frequency analysis and achieves improved EMI source location capability and accuracy.

Acknowledgements

This material is based upon work supported by the Air Force Research Laboratory (AFRL) under Contract No. FA9453-22-C-A127. Any opinions, findings and conclusions or recommendations expressed in this material are those of the authors and do not necessarily reflect the views of the AFRL.

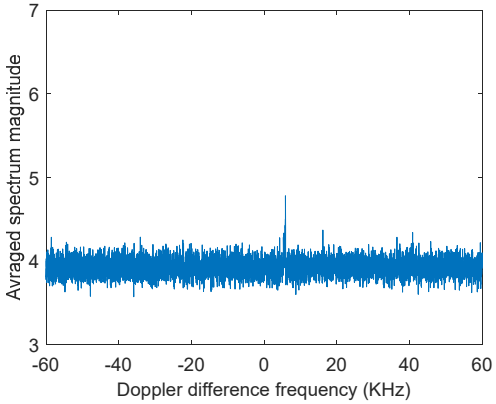

Figure 10. Averaged spectrum of the Doppler difference frequency (input INR = -30 dB, $x_v = -30$ km).

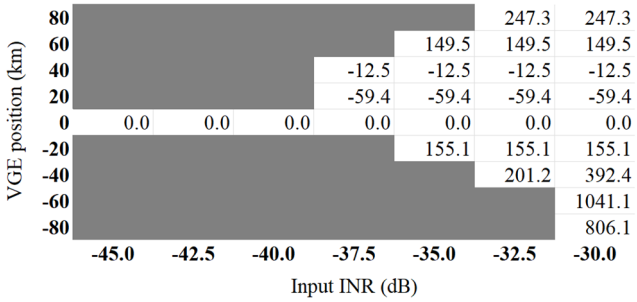

Figure 11. Estimated EMI position (in m) using a single VGR.

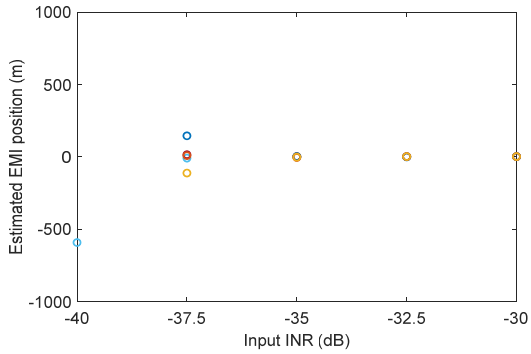

Figure 12. Estimated EMI position using 7 VGRs (5 trials).

References

[1] Y. Ding, "Blind Doppler estimation for satellite with interference EMI," in *Proc. Asilomar Conf. Signals, Syst., Comput.*, Pacific Grove, CA, Oct. 2022, pp. 1449–1455.

[2] D. Shen, G. Chen, and K. Pham, "Passive single satellite

geolocation of ground-based EMI sources," in *Proc. ION GNSS+*, Denver, CO, Sept. 2023, pp. 2384–2394.

[3] T. Pattison and S. I. Chou, "Sensitivity analysis of dual-satellite geolocation," *IEEE Trans. Aerosp. Electron. Syst.*, vol. 36, no. 1, pp. 56–71, 2001.

[4] K. C. Ho and W. Xu, "An accurate algebraic solution for moving source location using TDOA and FDOA measurements," *IEEE Trans. Signal Process.*, vol. 52, no. 9, pp. 2453–2463, 2004.

[5] S. Barbarossa, A. Scaglione, and G. B. Giannakis, "Product high-order ambiguity function for multi-component polynomial-phase signal modeling," *IEEE Trans. Signal Process.*, vol. 46, no. 3, pp. 691–708, 1998.

[6] I. Djurovic, M. Simeunovic, S. Djukanovic, and P. Wang, "A hybrid CPF-HAF estimation of polynomial-phase signals: Detailed statistical analysis," *IEEE Trans. Signal Process.*, vol. 60, no. 10, pp. 5010–5023, 2012.

[7] C. Ioana, Y. D. Zhang, M. G. Amin, F. Ahmad, G. Frazer, and B. Himed, "Time-frequency characterization of micro-multipath signals in over-the-horizon radar," in *Proc. IEEE Radar Conf.*, Atlanta, GA, May 2012, pp. 671–675.

[8] I. Djurovic and Y. D. Zhang, "Accurate parameter estimation of over-the-horizon radar signals using RANSAC and MUSIC algorithms," *Progress in Electromagnetics Research M*, vol. 67, pp. 85–92, April 2018.

[9] S. Zhang, M. S. Pavel, and Y. D. Zhang, "Crossterm-free time-frequency representation exploiting deep convolutional neural network," *Signal Process.*, vol. 192, no. 108372, pp. 1–14, March 2022.

[10] B. Boashash (Ed.), *Time-Frequency Signal Analysis and Processing, 2nd Edition*. Academic Press, 2015.

[11] M. A. Vazquez, A. Perez-Neira, D. Christopoulos, S. Chatzinotas, B. Ottersten, P.-D. Arapoglou, A. Ginesi, and G. Taricco, "Precoding in multibeam satellite communications: Present and future challenges," *IEEE Wireless Commun.*, vol. 23, no. 6, pp. 88–95, Dec. 2016.

[12] Y. D. Zhang and K. D. Pham, "Joint precoding and scheduling optimization in downlink multicell satellite communications," in *Proc. Asilomar Conf. Signals, Syst., Comput.*, Pacific Grove, CA, Nov. 2020, pp. 480–484.

[13] Y. D. Zhang, J. J. Zhang, M. G. Amin, and B. Himed, "Instantaneous altitude estimation of maneuvering targets in over-the-horizon radar exploiting multipath Doppler signatures," *EURASIP J. Adv. Signal Process.*, vol. 2013, no. 2013:100, pp. 1–13, May 2013.

[14] M. G. Amin and Y. D. Zhang, "Nonstationary jammer excision for GPS receivers using sparse reconstruction techniques," in *Proc. ION GNSS+*, Tampa, FL, Sept. 2014, pp. 3469–3474.

[15] Y. D. Zhang and B. Himed, "Multipath Doppler difference estimation in over-the-horizon radar," in *Proc. IEEE Radar Conf.*, Oklahoma City, OK, April 2018, pp. 693–697.

[16] S. Bhooshan, *Fundamentals of Analogue and Digital Communication Systems*, Springer, 2022.

BIOGRAPHIES

Yimin D. Zhang *received his B.Eng. degree from Northwest Telecommunications Engineering Institute (Now Xidian University), Xi'an, China, and received his Ph.D. degree in Applied Physics from the University of Tsukuba, Japan. He is currently an Associate Professor with the Department of Electrical and Computer Engineering, Temple University, Philadelphia, PA. His research interests include array signal processing, compressive sensing, machine learning, information theory, convex optimization, and time-frequency analysis with applications to radar, wireless communications, satellite navigation, and radio astronomy.*

Dr. Zhang is a Senior Area Editor for IEEE Transactions on Signal Processing and an Editor for Signal Processing. He has been selected as a 2024 IEEE Signal Processing Society Distinguisher Lecturer. He is a Fellow of IEEE, a Fellow of SPIE, and a Fellow of AAIA.

Yanwu Ding *received the B.Eng. degree from Southwest Jiaotong University, Chengdu, China, and the M.Sc. and Ph. D degrees from McMaster University, Hamilton, ON, Canada. She is currently with the Department of Electrical and Computer Engineering, Wichita State University, Wichita, KS, USA. Her research interests include signal processing in satellite and wireless communication systems.*

Dr. Khanh Pham *is a supervisory principal aerospace engineer at the Air Force Research Laboratory-Space Vehicles Directorate at Kirtland Air Force Base, New Mexico. He is an Adjunct Research Professor at the University of New Mexico Electrical and Computer Engineering researching control & game-theoretic operations research with assured satellite communications and resilient navigation. He is a Fellow of the Institute of Electrical and Electronics Engineers, the National Academy of Inventors, the Air Force Research Laboratory, the American Astronautical Society, the Society of Photo-Optical and Instrumentation Engineers, the Institution of Engineering and Technology, the Royal Aeronautical Society, the Royal Astronomical Society, Asia-Pacific Artificial Intelligence Association, and the International Association for the Advancement of Space Safety.*

In addition, his research interests have focused on statistical optimal control; decision analysis of adversarial systems; dynamic game decision optimization; security of cyber-physical systems; satellite cognitive radios; digital beamforming; military communications; alternative positioning, navigation, and timing; and control and coordination of large-scale dynamical systems. He is the author of two research monographs, including "Resilient Controls for Ordering Uncertain Prospects: Change and Response" (ISBN 978-3-319-08704-7, Springer 2014) and "Linear-Quadratic Controls in Risk-Averse Decision Making: Performance-Measure Statistics and Control Decision Optimization" (ISBN 978-1-4614-5078-8, Springer 2012). Lastly, he holds 34 US patents.

Dan Shen *received the B. S. in Automation from Tsinghua University in 1998, and the M. S. and Ph.D. in Electrical Engineering from the Ohio State University in 2003 and 2006; respectively. He is currently a chief scientist of the Intelligent Fusion Technology, Inc., Germantown MD. His research interest includes information fusion, data mining, signal processing, dynamic game theory and applications, cooperative control and decision making, cyber network security, and space communication systems.*

Genshe Chen *received the B. S. and M. S. in electrical engineering, PhD in aerospace engineering, in 1989, 1991 and 1994 respectively, all from Northwestern Polytechnical University, Xian, P. R. China.*

Currently Dr. Chen is the chief technology officer of Intelligent Fusion Technologies, Inc, Germantown, MD. His research interests include cooperative control and optimization for military operations, Target tracking and multi-sensor fusion, Cyber Security, C4ISR, Electronic Warfare, Digital signal processing and image processing, Game theoretic estimation and control, Bayesian network, Influence diagram, robotics, and Human-Cyber-Physical system.